Structural Studies of the HIV-1 Accessory Protein Vpu in Langmuir Monolayers: Synchrotron X-ray Reflectivity

Songyan Zheng,* Joseph Strzalka,* Che Ma,* Stanley J. Opella,* Benjamin M. Ocko,† and J. Kent Blasie*
*Department of Chemistry, University of Pennsylvania, Philadelphia, Pennsylvania 19104-6323, and †Department of Physics, Brookhaven National Laboratory, Upton, New York 11973, USA

ABSTRACT Vpu is an 81 amino acid integral membrane protein encoded by the HIV-1 genome with a N-terminal hydrophobic domain and a C-terminal hydrophilic domain. It enhances the release of virus from the infected cell and triggers degradation of the virus receptor CD4. Langmuir monolayers of mixtures of Vpu and the phospholipid 1,2-dilignoceroyl-*sn*-glycero-3-phosphocholine (DLgPC) at the water–air interface were studied by synchrotron radiation-based x-ray reflectivity over a range of mole ratios at constant surface pressure and for several surface pressures at a maximal mole ratio of Vpu/DLgPC. Analysis of the x-ray reflectivity data by both slab model-refinement and model-independent box-refinement methods firmly establish the monolayer electron density profiles. The electron density profiles as a function of increasing Vpu/DLgPC mole ratio at a constant, relatively high surface pressure indicated that the amphipathic helices of the cytoplasmic domain lie on the surface of the phospholipid headgroups and the hydrophobic transmembrane helix is oriented approximately normal to the plane of monolayer within the phospholipid hydrocarbon chain layer. At maximal Vpu/DLgPC mole ratio, the tilt of the transmembrane helix with respect to the monolayer normal decreases with increasing surface pressure and the conformation of the cytoplasmic domain varies substantially with surface pressure.

INTRODUCTION

The human immunodeficiency virus type 1 (HIV-1) genome encodes six accessory proteins (Emerman and Malim, 1998). Vpu, one of those accessory proteins, is an 81 amino acid phosphoprotein with a N-terminal hydrophobic domain and a C-terminal hydrophilic domain. Analysis of Vpu's amino acid sequence has suggested a putative structure of Vpu consisting of a hydrophobic domain containing 27 amino acids that forms a transmembrane α-helix inside the hydrocarbon core of the membrane and a hydrophilic domain containing 54 amino acids that protrudes from the membrane in the form of linked amphipathic α-helices.

Studies of the biological function of Vpu have demonstrated that it is involved in two different activities, namely the enhancement of the release of virus from the infected cell surface (Schubert et al., 1996) and the triggering of the degradation of the CD4 molecule in the endoplasmic reticulum (ER) (Willey et al., 1992; Schubert and Strebel, 1994). The enhancement of virus release is dependent on the transmembrane domain of Vpu, which also exhibits nonspecific cation channel activity (Ewart et al., 1996). In the case of degradation of CD4, the specific virus receptor on the cell surface, the hydrophilic domain of Vpu interacts with the cytoplasmic domain of CD4, thereby disrupting the gp 160/CD4 interaction to form a stable complex in the ER, thereby triggering the proteolysis of CD4 (Chen et al., 1993; Maldarelli et al., 1993; Lenburg and Landau, 1993; Schubert et al., 1994; Bour et al., 1995). As a consequence, Vpu induces a release of gp 160, a virus envelope glycoprotein precursor, from CD4 otherwise trapped in the ER to thereby increase the rate of virus particle secretion.

Studies of the secondary structure of the submolecular fragments of Vpu by NMR spectroscopy have indicated that the hydrophilic domain possesses two distinct α-helices in KH_2PO_4 buffer (pH 3.5) (Wray et al., 1995) and trifuoroethanol (TFE) (Federau et al., 1996), and three α-helices in NaCl and KH_2PO_4 buffer (pH 7.0) solutions (Willbold et al., 1997). A recent study of phospholipid detergent micelles containing full-length Vpu has indicated that the hydrophobic domain is a single α-helix and the hydrophilic domain contains two α-helices; the two domains appear to fold independently in membrane environments and not interact strongly with each other (Marassi et al., 1999). Solid-state NMR experiments on oriented phospholipid multilayers containing full length Vpu have indicated that the hydrophobic domain is a transmembrane α-helix oriented approximately normal to the bilayer plane, with a tilt angle at $\sim$15°, whereas the hydrophilic α-helices are oriented parallel to bilayer plane (Marassi et al., 1999). Furthermore, the nonspecific cation channel activity of Vpu and its enhancement of virus release is due to Vpu's transmembrane domain (Marassi et al., 1999). Note that, with regard to the physiological environment of Vpu, the water space between adjacent bilayers in oriented lipid multilayers is generally relatively small and potentially restrictive, the curvature in detergent micelles is generally substantially larger than that of a lipid bilayer, and Vpu is not unidirectionally oriented in either, as it is in a natural membrane environment.

Conversely, Langmuir monolayers of Vpu/phospholipid mixtures provide an infinite bulk water subphase, a planar phospholipid monolayer environment (but not a bilayer; see below), a unidirectional vectorial orientation of Vpu, and

Received for publication 28 June 2000 and in final form 19 January 2001.
Address reprint requests to J. Kent Blasie, Univ. of Pennsylvania, Dept. of Chemistry, 231 South 34th St., Philadelphia, PA 19104-6323. Tel.: 215-898-6208; Fax: 215-898-6242; E-mail: jkblasie@sas.upenn.edu.

0006-3495/01/04/1837/14 $2.00

the possibility of variation of both the Vpu/phospholipid ratio and the surface pressure independently (noting that pressure and temperature are both important thermodynamic variables). Suitable techniques such as x-ray reflectivity, grazing-incidence x-ray diffraction (GIXD) and neutron reflectivity can be used to investigate the structure of both Vpu and its environment in Langmuir monolayers (Als-Nielsen et al., 1994). Specular x-ray reflectivity can provide the localization of Vpu within the profile structure of the monolayer, off-specular reflectivity and GIXD can provide both the aggregation (or oligomeric) state of Vpu and the intermolecular ordering of phospholipid within the plane of the monolayer, and neutron reflectivity with specifically deuterated amino acids can provide a key set of distance measurements constraining the three-dimensional (3D) structure of Vpu within the monolayer (Blasie and Timmins, 1999). Although the environment for the transmembrane domain of Vpu within such Langmuir monolayers is not that provided by a lipid bilayer, it is well established that physical–chemical studies of model systems based on lipid monolayers (both as Langmuir monolayers at the air/water interface and as supported monolayers on alkylated solid substrates), and on lipid bilayers, can provide substantial insight into the structure, dynamics, and phase behavior of the more complex lipid bilayers found in biological membranes (Möhwald, 1995). Furthermore, membrane proteins are now being incorporated onto and into such lipid monolayers in physical–chemical studies of the role of lipid–protein interactions in the structure and function of membrane proteins (Shapovalov et al., 1999; Schwarz and Taylor, 1999; Ionov et al., 2000; Maierhofer et al., 2000). In addition, such Langmuir monolayers containing the unidirectionally oriented membrane protein are an important precursor to forming a lipid bilayer maintaining the vectorial orientation of the protein via Langmuir–Blodgett techniques.

In this paper, we present the initial experimental results from the synchrotron radiation-based x-ray reflectivity study of Langmuir monolayers of a pure phospholipid, whose hydrocarbon chain length was selected to nearly match the length of Vpu's hydrophobic helix, and its mixtures with Vpu at the water–air interface. The x-ray reflectivity data as a function of decreasing lipid/protein mole ratio clearly indicates the mixing of the two components in the plane of the Langmuir monolayer in spite of the saturation of the long lipid hydrocarbon chains, consistent with the disordering of gel-phase domains as demonstrated directly by GIXD. The x-ray reflectivity data from these monolayers were analyzed by two totally independent methods, both using the first Born approximation. The first was a slab model-refinement procedure, which uses a minimal number of slabs of constant density, where the parameters describing the slabs are varied to improve the agreement between the experimental data and that predicted by the model. Here, the Vpu contribution was treated as a systematic perturbation to the pure lipid monolayer profile structure as a function of increasing protein/lipid mole ratio. A second model-independent box-refinement procedure used only the finite extent of the monolayer structure normal to the air–water interface, which is known experimentally. The excellent agreement of the profiles obtained from the two methods firmly establishes the so-determined electron density profiles of the monolayers. Comparison of the electron density profiles as a function of increasing Vpu/phospholipid mole ratio at a constant, relatively high surface pressure clearly indicates the contribution of the protein to the monolayer. A molecular model of the Vpu protein within a phospholipid monolayer at the water–air interface consistent with the electron density profiles is presented. The experimental results also show that the profile structure of Vpu can be substantially altered by varying the surface pressure of mixed monolayers at the maximal Vpu/phospholipid mole ratio.

MATERIALS AND METHODS

Vpu purification

The detailed procedure for the cloning, expression, and purification, as well as the biological activities of Vpu will be published elsewhere. Briefly, *Escherichia coli* strain BL21 (DE3) cells were transformed with the vectors carrying the Vpu gene and grown in minimal media. Nickel affinity chromatography (HisBind Resin, Novagen) enabled the separation of the His tagged fusion protein from other proteins in cell lysate. Cyanogen bromide was used to cleave Vpu from the fusion partner (Gross and Witkop, 1961). The Vpu polypeptides have the two Met residues in the Vpu sequence changed to Leu to facilitate cyanogen bromide cleavage of the fusion protein systems used for expression and purification. Reverse-phase high-performance liquid chromatography was used to isolate Vpu. The purity and integrity of Vpu was confirmed by mass spectrometry. The biological activity of this double mutant protein is the same as that of authentic Vpu (unpublished results). The sequence of cleaved recombinant full-length Vpu polypeptide is QPIQIAIVAL VVAIIIAIVV WSIVIIEYRK ILRQRKIDRL IDRLIERAED SGNESEGEIS ALVELGVELG HHAPWDVDDL.

Choice of phospholipid

The phospholipid used in these studies was 1,2-dilignoceroyl-s*n*-glycero-3-phosphocholine (abbreviated herein as DLgPC, chromatographically pure, from Avanti Polar Lipids, Inc., Alabaster, AL), which has C24 saturated hydrocarbon chains, the longest chain-length commercially available. This phospholipid and the phospholipids used in both short-chain micelles and longer-chain oriented multilayers for the NMR experiments briefly described in the introduction have identical polar headgroups, making our data as comparable as possible to the NMR experiments, at least with regard to the headgroup. However, because the length of Vpu's hydrophobic α-helix is 34.5 Å containing 23 residues (Willbold et al., 1997), the use of DLgPC provides a nonpolar core for the host phospholipid monolayer whose maximal thickness (29.4 Å for untilted, fully extended, all-trans chains) roughly matches the length of Vpu's hydrophobic α-helix, although the N-terminus of the transmembrane helix would be only in a moist helium environment in the Langmuir monolayer instead of that provided by phospholipid headgroups and water in a bilayer. The fact that the diacyl hydrocarbon chains are saturated for DLgPC is mitigated by our demonstration that the DLgPC and Vpu mix in the Langmuir mono-

layers, which precludes their providing a gel-phase environment for the Vpu transmembrane helix at the higher protein/lipid mole ratios and the lower surface pressures used in this study, as described in the Results section. Vpu and DLgPC were dissolved in the desired mole ratio in a 3:1 chloroform:methanol solution. Monolayers were prepared by spreading pure phospholipid and mixtures of Vpu/phospholipid onto Millipore filtered water subphase. The monolayers were kept at a constant temperature of 20°C during the x-ray reflectivity measurements.

Langmuir trough

A custom built Langmuir trough, fabricated from a copper block and coated with Teflon, contained the water subphase and the spread monolayer. The temperature of the water subphase was controlled by cooled water circulation in the copper block and was measured with a resistance thermometer probe. Surface pressure was measured by a Wilhelmy plate and controlled by a movable barrier with feedback. Because high quality x-ray reflectivity data can only be obtained from Langmuir monolayers when the aqueous subphase surface is relatively smooth, the Langmuir trough sat on a vibration isolation stage in the liquid surface spectrometer described below, a delay time of several seconds was used between any motion of the spectrometer and data collection, and a flat smooth silicon block was also submerged slightly below the water surface to damp long wavelength excitations in the local height of the water surface. During the x-ray reflectivity measurements, moist helium gas was circulated inside the trough to replace the air, thereby reducing the x-ray background scattering.

Liquid-surface spectrometer

The x-ray reflectivity experiments were performed on beamline X-22B at the National Synchrotron Light Source at Brookhaven National Laboratory, Upton, New York. Details of the liquid surface spectrometer have been reported elsewhere (Als-Nielsen and Pershan, 1983; Braslau et al., 1988; Ocko et al., 1997). Here we give only a brief description. The synchrotron x-ray source was a bending-magnet in the electron storage ring operating at an energy of 2.8 GeV and currents of 150–250 mA. Monochromatic x-rays were obtained with a horizontally reflecting Si (111) crystal monochromator to provide a wavelength $\lambda = 1.546$ Å. X-rays were reflected downward onto the horizontal liquid-surface through a Ge (111) crystal to provide angle of incidence α. Incident beam slits were set to collect the full horizontal beamwidth and vertically to limit the beam footprint on the liquid surface. A scintillation detector recorded the scattering from a thin Kapton film in the incident beam to provide an incident beam flux monitor. The specularly reflected beam from the liquid surface was measured at an angle β with respect to the liquid surface with another scintillation detector for $\alpha = \beta$ in the vertical scattering plane at $2\theta_{xy} = 0°$. Scattered beam slits were set to accept the full specularly reflected beam. Off-specular background was measured at $\alpha = \beta$ with $2\theta_{xy} = \pm 0.3°$. The difference (specular minus off-specular background) provided the reflectivity $R(q_z)$ for photon momentum transfer q_z perpendicular to liquid surface with $q_z = (4\pi/\lambda)\sin\alpha$.

DATA ANALYSIS

The normalized reflectivity $R(q_z)/R_F(q_z)$ from a liquid surface arises from, in the first Born approximation, the modulus square of the Fourier transform of the derivative $d\rho(z)/dz$ of the electron density profile $\rho(z)$ across the air–water interface averaged over the in-plane coherence length of the incident x-rays (Als-Nielsen and Pershan, 1983; Helm et al., 1991), namely

$$\frac{R(q_z)}{R_F(q_z)} = \left| (\rho_\infty^{-1}) \int \left[\frac{d\rho(z)}{dz} \right] \exp(iq_z' z)\, dz \right|^2 \equiv |F(q_z')|^2, \qquad (1)$$

where $R_F(q_z)$ is Fresnel reflectivity from a single infinitely sharp (ideal) interface, the electron density of the semi-infinite bulk subphase is ρ_∞, and q_c is q_z at the critical angle for the subphase α_c. This expression, Eq. 1, becomes progressively less valid as q_z approaches q_c, which is mitigated to some extent by the use of q_z' (Lösche et al., 1993).

The traditional model-refinement method of analyzing the normalized reflectivity data from Langmuir monolayers uses a minimal number of slabs of constant electron density expressed in a simple analytic form with a finite set of parameters and a nonlinear least-squares fitting of the model parameters to the measured reflectivity data via Eq. 1. The initial parameters of this model profile must be carefully chosen because most algorithms for implementing the fitting, including the Marquardt algorithm (Bevington and Robinson, 1992) used here, are notorious for finding only the local minimum in the χ^2 hypersurface nearest the initial model. Nevertheless, this approach has been effectively applied to the analysis of the normalized x-ray reflectivity obtained from phospholipid monolayers (Helm et al., 1987, 1991) and fatty-acid monolayers (Kjaer et al., 1989) and polymers (Majewski et al., 1998) at the water–air interface and organic self-assembled monolayers chemisorbed on silicon (Tidswell et al., 1990). Recently, our group has analyzed normalized x-ray reflectivity from Langmuir monolayers of synthetic model peptides and mixtures of these peptides with phospholipids (Strzalka, 2000).

The so-called box-refinement method provides an iterative, model-independent approach to obtaining the phase of (and thereby recovering the electron density profile that gave rise to) the scattered intensity collected in a reflectivity experiment (Stroud and Agard, 1979; Makowski, 1981). It has been used successfully to solve for the electron density profile structure of a variety of lipid and protein thin films on solid supports (Skita et al., 1986a,b). To apply this method, two criteria must be met. First, the structure of interest must be of finite extent. This is true for Langmuir films in the direction normal to the monolayer–air interface, just as it is for the ultrathin films on solid supports. Second, the data being analyzed must be in the kinematical limit in which the incident beam is scattered only weakly. In this limit, the scattering potential and the scattering amplitude are Fourier transform/inverse Fourier transform pairs (the first Born approximation). Eq. 1 shows that, in the usual reflectivity formalism, this is true of the derivative of the electron density profile and $F(q_z')$ where $|F(q_z')|^2$ is the normalized reflectivity $R(q_z)/R_F(q_z)$ represented in q_z'-space. Because the derivative of the electron density profile is also finite in extent, we can apply the box-refinement algorithm to reflectivity data to recover this function and then integrate to obtain the electron density profile itself. If the results so obtained agree with the electron density profile from the model refinement approach described above, the two methods together provide an independent cross-check on the convergence of the analysis to the global best fit, and therefore to the overall physical correctness of the electron density profile so-obtained.

Because the box refinement method is not well known in the analysis of (x-ray or neutron) reflectivity data, it will be briefly described here. The algorithm provides a method for transforming an initial arbitrary trial profile structure into a profile structure that correctly predicts the experimentally observed normalized reflectivity to within experimental error. The heart of the algorithm is the box constraint: the correct solution for $d\rho(z)/dz$ will be finite in extent, namely zero outside a box of length L, and of the same size as the actual profile structure $\rho(z)$. This key constraint can be obtained from the experimental data without any assumptions by computing the unique inverse Fourier transform of the normalized reflectivity data itself expressed in q_z'-space as $|F_{exp}(q_z')|^2$. This operation yields the autocorrelation function of the derivative of the electron density profile (the so-called generalized Patterson function). If the monolayer profile structure has a thickness L, the significant oscillations in the generalized Patterson function will die out for z beyond $\pm L$, because correlations within a structure cannot extend over distances larger than the structure itself.

The box constraint is first input into the algorithm. It is usually relaxed to be somewhat larger than L itself, but the pressure toward convergence diminishes as the constraint is increased well beyond L. We also input the

square root of the experimental normalized reflectivity $|R_{exp}(q_z)/R_F(q_z)|$, which gives the modulus of the Fourier transform of the derivative of the electron density distribution $d\rho/dz$ expressed in q_z'-space as $|F_{exp}(q_z')|$. We start the algorithm with an arbitrary trial structure, $(d\rho/dz)_0$ (a clearly incorrect choice leads to the most convincing result), and compute its Fourier transform. We discard the modulus of the Fourier transform but retain the resulting phase function, $\phi_1(q_z')$. We use $\phi_1(q_z')$ to compute the inverse Fourier transform of $|F_{exp}(q_z')|$ and obtain a new structure, $(d\rho/dz)_1$. At this point, we apply the box constraint. The function $(d\rho/dz)_1$ is truncated to remove the portions beyond the limits $-L/2 < z < +L/2$ to obtain $(d\rho/dz)_{1t}$. Now we compute the Fourier transform of $(d\rho/dz)_{1t}$ to obtain a new phase function $\phi_2(q_z')$. We then use this new phase $\phi_2(q_z')$ to compute the inverse Fourier transform of $|F_{exp}(q_z')|$ and obtain a new structure, $(d\rho/dz)_2$, truncate to obtain $(d\rho/dz)_{2t}$, Fourier transform to obtain a new phase function $\phi_3(q_z')$, and so on. We check the progress of the iteration of $\phi_n(q_z')$ by comparing the modulus square of the Fourier transform of $(d\rho/dz)_n$ with $|F_{exp}(q_z')|^2$. The algorithm converges when $|F_{exp}(q_z')|^2$ and the modulus square of the Fourier transform of $(d\rho/dz)_n$ agree to within the counting statistics noise in the former, and there is little change between $(d\rho/dz)_{n-1}$ and $(d\rho/dz)_n$. Finally, we can integrate $(d\rho/dz)_n$ to obtain the fully converged electron density profile itself $\rho_n(z)$.

RESULTS

Isotherms

Monolayers of pure DLgPC and mixtures of Vpu/DLgPC were spread from 3:1 chloroform-methanol solutions on a pure water subphase at 20°C. Surface pressure-area isotherms for pure DLgPC and mixed Vpu/DLgPC are shown in Fig. 1. The isotherm for the pure DLgPC monolayer is relatively featureless for larger areas/molecule with sharply increasing pressure only as the minimum area/molecule of ~ 40 Å^2 is approached. In contrast, while the mixed monolayers show systematic effects of increasing Vpu content, they all possess an inflection point at a surface pressure of ~ 20 mN/m. This additional feature may represent a structural reorganization in the mixed monolayers as discussed below (See Results and Discussion).

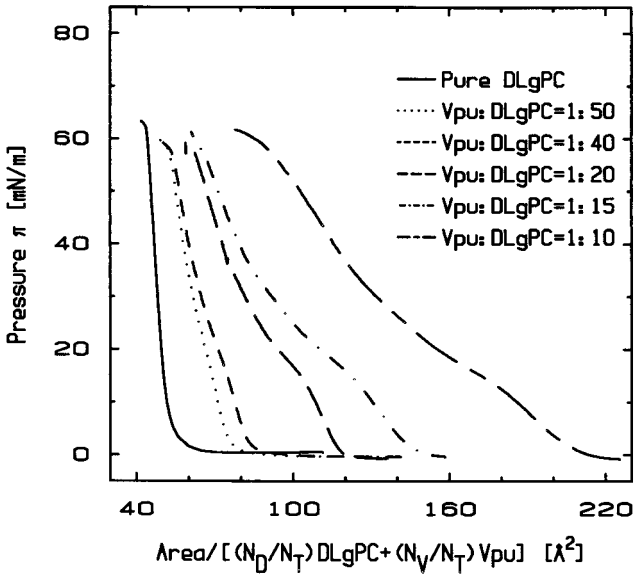

FIGURE 1 Surface pressure/area isotherms of pure DLgPC and mixed Vpu/DLgPC monolayers for the various mole ratios indicated on a pure water subphase at $T = 20$°C. The abscissa is expressed in terms of the sum of the fractional areas occupied by the DLgPC and Vpu molecules in the plane of the monolayer (N_D = moles DLgPC, N_V = moles Vpu, $N_T = N_D + N_V$).

The systematic changes in the isotherms for the mixed Vpu/DLgPC monolayers with increasing Vpu content demonstrate that Vpu molecules occupy a substantial fraction of the area on water surface. This result indicates the presence of a strong affinity of the Vpu molecule for the surface, which may be enhanced by the lateral interactions with DLgPC in the plane of the monolayer, that is, Vpu cannot be simply submerged below the DLgPC monolayer in the water subphase.

Reflectivity data

Fig. 2 *A* shows the normalized reflectivity $R(q_z)/R_F(q_z)$ (*open circles*) for the monolayers of pure DLgPC and mixtures of Vpu/DLgPC at mole ratios of 1:50, 1:40, 1:20, 1:15, and 1:10 at the surface pressure of 45 mN/m. Qualitatively, the systematic decrease in the period of the oscillation in $R(q_z)/R_F(q_z)$ with increasing mole ratio simply indicates an increase in the overall thickness of monolayer. This systematic effect also suggests that lateral inhomogeneities in the mixed monolayers are smaller than the lateral coherence length $\sim 10^4$ Å of the synchrotron x-rays (Helm et al., 1991). The presence of such lateral inhomogeneities larger than the lateral coherence length would lead to an incoherent superposition of the normalized reflectivities for each type of domain. As a result, the amplitudes of their respective maxima would simply increase for one type and decrease for the other with a systematic change of mole ratio, in contrast to the behavior observed. Thus, the two components are mixing in the plane of the Langmuir monolayers on this length scale over this range of mole ratios. Furthermore, direct GIXD measurements demonstrate that the well-ordered hexagonal packing of DLgPC hydrocarbon chains in the plane of the monolayer characteristic of the gel phase for the pure phospholipid already becomes substantially less ordered for Vpu/DLgPC ratios of 1:50 and smaller, and is completely disordered (Helm et al., 1991; Als-Nielsen et al., 1994) for Vpu/DLgPC ratios of 1:20 and larger, as shown in Figure 2 *B*. These results are consistent with the mixing of the two components on the molecular length scale over the full range of mole ratios investigated here. Finally, the progressive decrease in the amplitude of the second and third maxima at higher q_z relative to the first implies a general increase in interfacial roughnesses or widths with increasing Vpu mole ratio. At this relatively high surface pressure, there is little possibility for the DLgPC molecules to gain more extension in the monolayer profile (i.e., they are already approaching their minimum area). The increases in overall thicknesses of the mixed

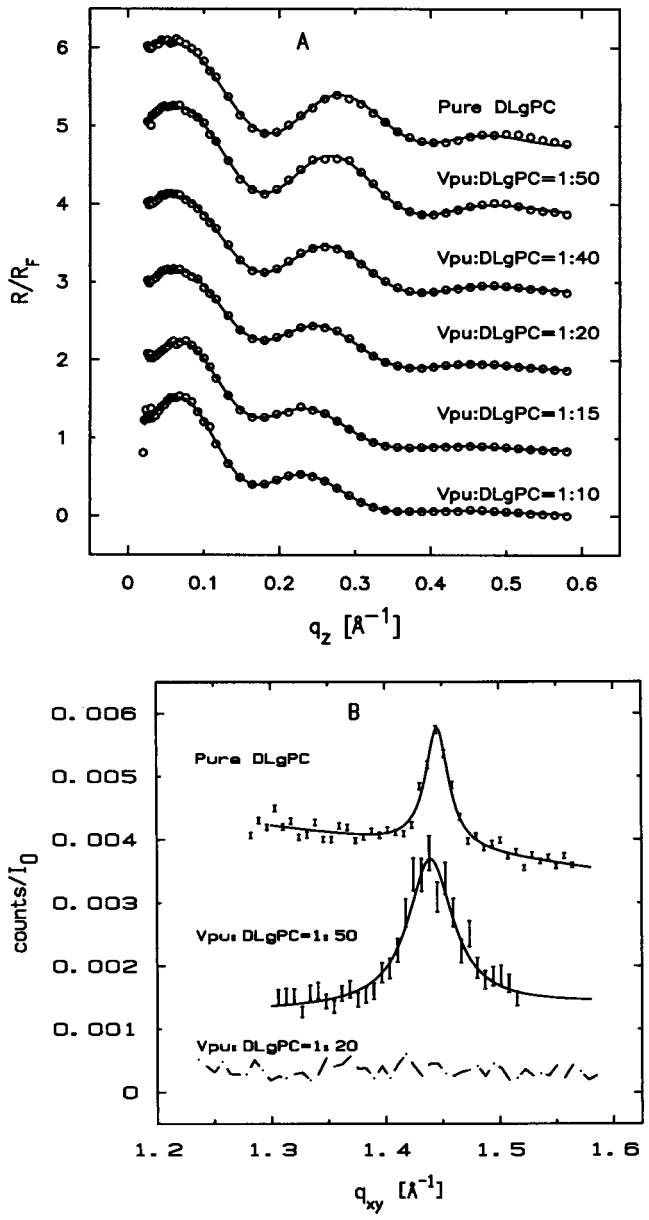

FIGURE 2 (*A*) Normalized reflectivity $R(q_z)/R_F(q_z)$ data (*open circles*) as a function of photon momentum transfer q_z and the best fits (*solid lines*) resulting from the model refinement analysis for various mole ratios of Vpu/DLgPC indicated, all at a surface pressure of 45 mN/m and $T = 20°C$. (*B*) Corresponding grazing-incidence x-ray diffraction (GIXD) data from the Langmuir monolayers of pure DLgPC (*top*) and from mixed monolayers with Vpu/DLgPC mole ratios of 1:50 (*middle*) and 1:20 (*bottom*). The single diffraction peak at $q_{xy} = 1.446$ Å^{-1} for the pure DLgPC is characteristic of the hexagonal ordering of hydrocarbon chains in the plane of the monolayer for the gel phase, with a lattice spacing of 4.35 Å and an area/molecule of 43.7 Å^2, whose width (FWHM) indicates a correlation length of 81 ± 8 Å, describing the exponential decay of chain–chain positional correlations in the monolayer plane (Helm et al., 1991; Als-Nielsen et al., 1994). This peak diminishes in amplitude and increases in width for the Vpu/DLgPC mole ratio of 1:50, indicating a decreased correlation length of 42 ± 6 Å, and disappears into the noise upon reaching a mole ratio of 1:20, indicating a further decreased correlation length of less than 12–20 Å (i.e., 3–5 lattice spacings) and the destruction of the intermolecular ordering of the gel phase. These changes are due to mixing of the protein and lipid components of the monolayer on the molecular length scale over the full range of mole ratios studied here. Note that the continuous curves are the best fits of a Lorentzian line shape to the GIXD data, the data for the three monolayers have been arbitrarily offset vertically for clarity, and the ordinate scale applies to the two mixed monolayer cases.

monolayers are therefore due to the profile structure of Vpu, namely the projection of its 3D structure in the monolayer onto the normal to the plane of the monolayer.

Figure 3 shows the normalized reflectivity $R(q_z)/R_F(q_z)$ (*open circles*) for the pure DLgPC and a 1:10 mole ratio of Vpu/DLgPC at pressures of 13 mN/m, 45 mN/m, and 55 mN/m. Compared to pure DLgPC, the maxima in the normalized reflectivity $R(q_z)/R_F(q_z)$ for the mixed monolayers all decrease in the period of the oscillation for all three pressures. These changes must also arise from Vpu's profile structure. In addition, the amplitudes of the second and third maxima in $R(q_z)/R_F(q_z)$ at higher q_z for both pure DLgPC and the mixed monolayers are seen to decrease steadily with increasing surface pressure relative to that of the first maxima. This suggests that higher surface pressure progressively roughens or broadens all interfaces in the profile structure of the monolayer, namely between the subphase and the headgroups, the headgroups and the hydrocarbon chains, and the hydrocarbon chains and air.

Model refinement

The slab model-refinement approach to analyze the x-ray reflectivity data is strongly dependent on the initial slab model profile structure for the monolayer. Based on prior studies of Langmuir monolayers of pure phospholipids with shorter hydrocarbon chain lengths (as well as much earlier studies of phospholipid bilayers within oriented multilayers) (Helm et al., 1987, 1991; Kjaer et al., 1989), the profile structure of a DLgPC monolayer can be adequately described by a two-slab model (i.e., a step-function profile containing two distinct steps of constant electron density), one slab containing the polar headgroups and the other containing the hydrocarbon chains. Such a model is readily parameterized in terms of the electron densities and widths of the two slabs (or steps) relative to the electron density of the subphase and air, and by the roughness or width (σ) of the interfaces between adjacent slabs (or steps) as described by a Gaussian factor $e^{-\sigma^2 q^2}$ for each interface. Note that the roughness or width of all interfaces in the slab model were constrained to be greater than or equal to the roughness of the initial water–air interface, e.g., ~3 Å.

The initial model profile structure for fitting the x-ray reflectivity data from the mixed monolayers of Vpu/DLgPC was then taken to be exactly the same as that used to refine the electron density profile for the pure DLgPC monolayer, thus treating the Vpu as a perturbation of the host DLgPC

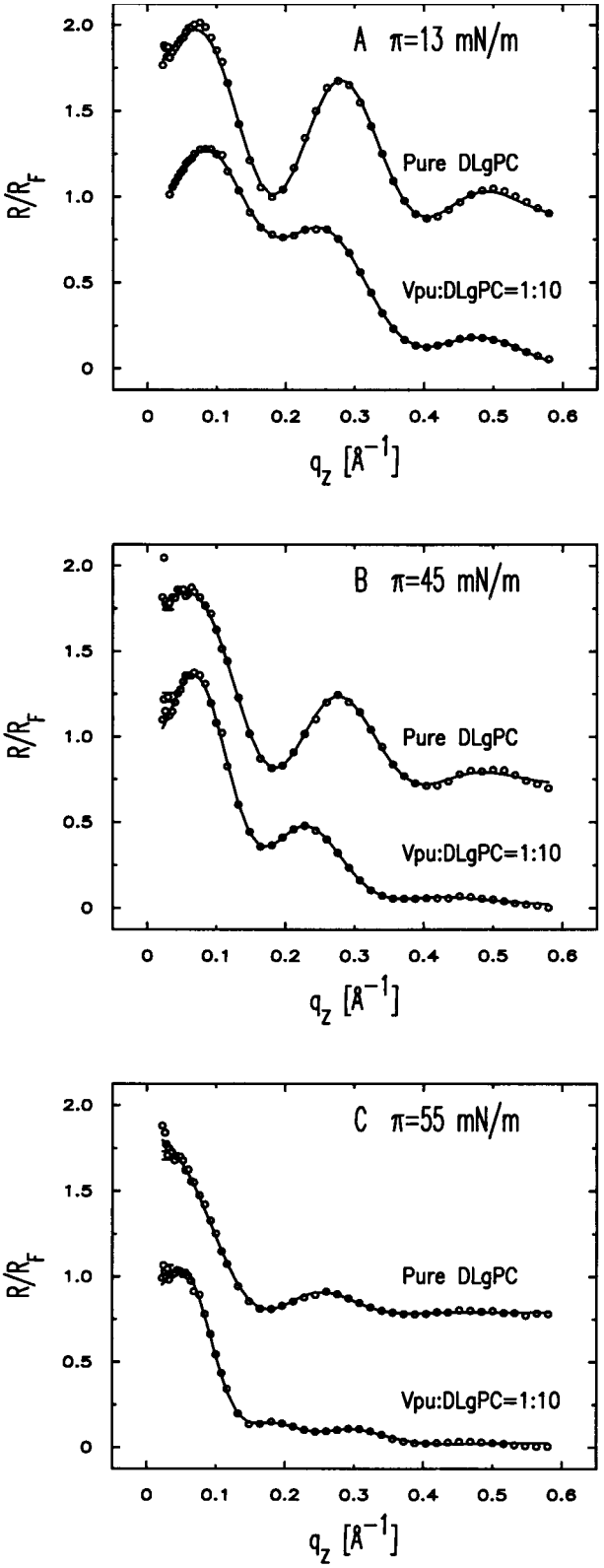

FIGURE 3 Normalized reflectivity $R(q_z)/R_F(q_z)$ data (*open circles*) as a function of photon momentum transfer q_z and the best fits (*solid lines*) resulting from the model refinement analysis for the 1:10 mole ratio of Vpu/DLgPC at $T = 20°C$ and surface pressures of (*A*) 13 mN/m; (*B*) 45 mN/m; and (*C*) 55 mN/m. Data sets have been offset for charity.

monolayer. This is justified by the systematic changes observed in the normalized reflectivity data for increasing Vpu/DLgPC mole ratio as shown in Fig. 2 and described above. By using the same initial model profile structure for all Vpu/DLgPC mole ratios, all of the profiles for the various mole ratios are equally biased toward the pure DLgPC profile structure. Fig. 2 also shows the best fits (*solid lines*) to the normalized reflectivity $R(q_z)/R_F(q_z)$ (*open circles*) resulting from this model refinement for the monolayers of pure DLgPC and mixtures of Vpu/DLgPC at mole ratios of 1:50, 1:40, 1:20, 1:15, and 1:10 at the surface pressure of 45 mN/m.

The electron density profile corresponding to the best fit for pure DLgPC is shown in Fig. 4. To obtain a reasonable estimate of the thickness of the polar headgroup and hydrocarbon chain layers from this profile, given the roughness of the interfaces, we used half maximal points in the profile as shown in Fig. 4. The average thickness of the polar headgroup (*A*) and hydrocarbon chain (*B*) layers were thereby found to be 8.6 and 24.5 Å, respectively. The thickness of the headgroup layer agrees with previous work that indicates a thickness perpendicular to the water surface of 7.5∼9 Å (Helm et al., 1987). For all-trans hydrocarbon chains, the hydrocarbon chain layer thickness suggests an average tilt angle of 30∼35° with respect to the normal to the monolayer plane.

Figure 5 illustrates the obvious differences between the electron density profile of pure DLgPC and the various mixtures of Vpu/DLgPC with increasing mole ratio by superposing the six electron density profiles all refined from the same initial model profile as described above. Note that

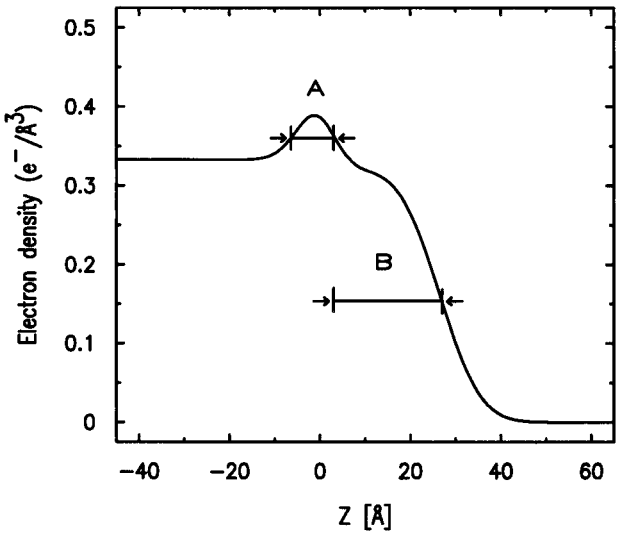

FIGURE 4 Electron density profile corresponding to the best fit from the model refinement analysis for pure DLgPC at a surface pressure of 45 mN/m and $T = 20°C$. The inflection points used to determine the average thicknesses (FWHM) of the (*A*) polar headgroup and (*B*) hydrocarbon chain layers are indicated.

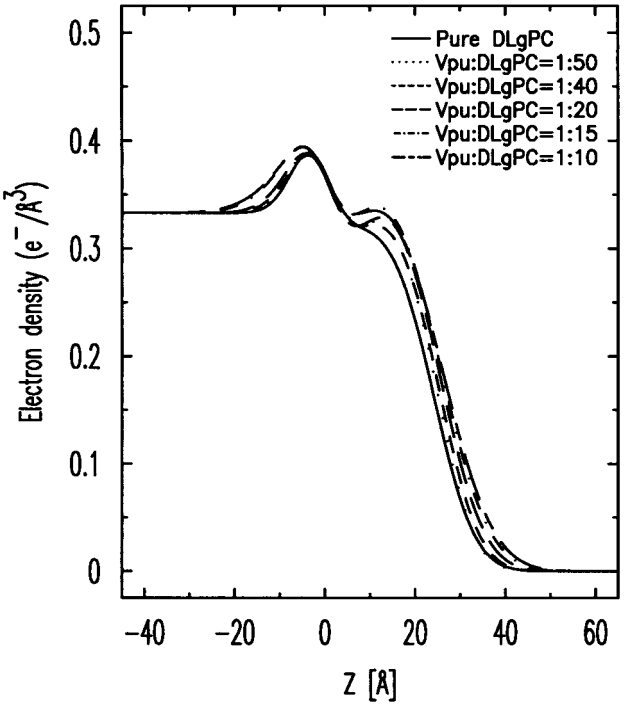

FIGURE 5 Electron density profiles corresponding to the best fits from the model refinement analysis for the various mole ratios of Vpu/DLgPC indicated at a surface pressure of 45 mN/m and $T = 20°C$.

the $z = 0$ Å origin for each of the so-derived electron density profiles is arbitrary; here the profiles have been superimposed such that their hydrocarbon–water interfaces occur at $z = 0$ Å based on the assumption that this is their only common feature.

In Fig. 3, we also show the best fits (*solid line*) to the normalized reflectivity $R(q_z)/R_F(q_z)$ (*open circles*) resulting from the model refinement for the pure DLgPC and a 1:10 mole ratio of Vpu/DLgPC at pressures of 13, 45, and 55 mN/m. The pressure-dependent changes in the electron density profiles corresponding to the best fits for DLgPC and the 1:10 mole ratio mixture of Vpu/DLgPC at pressures of 13 mN/m (*A*), 45 mN/m (*B*) and 55 mN/m (*C*) are shown in Fig. 6. Here also the same $z = 0$ Å origin choice has been used as described above.

Box refinement

In x-ray reflectivity, only the modulus of the Fourier transform of the derivative of the electron density profile is available from the normalized $R(q_z)/R_F(q_z)$ data and the corresponding phase necessary to uniquely invert the data to obtain the derivative and its integral, the electron density profile itself, is not. The box-refinement procedure generally converges to a phase solution fully consistent with the measured reflectivity data to within its errors. Because it is not an analytic procedure (in the mathematical sense), box-

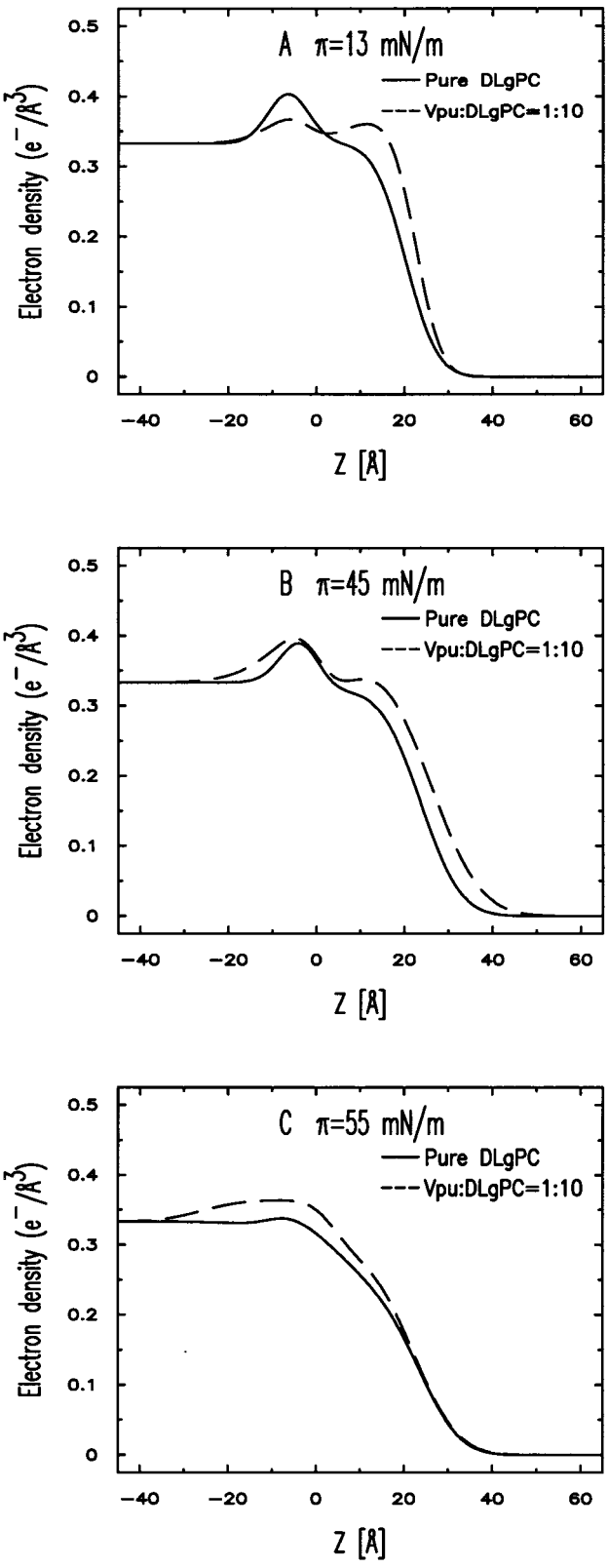

FIGURE 6 Electron density profiles corresponding to the best fits resulting from the model refinement analysis for the 1:10 mole ratio of Vpu/DLgPC at $T = 20°C$ and surface pressures of (*A*) 13 mN/m, (*B*) 45 mN/m, and (*C*) 55 mN/m.

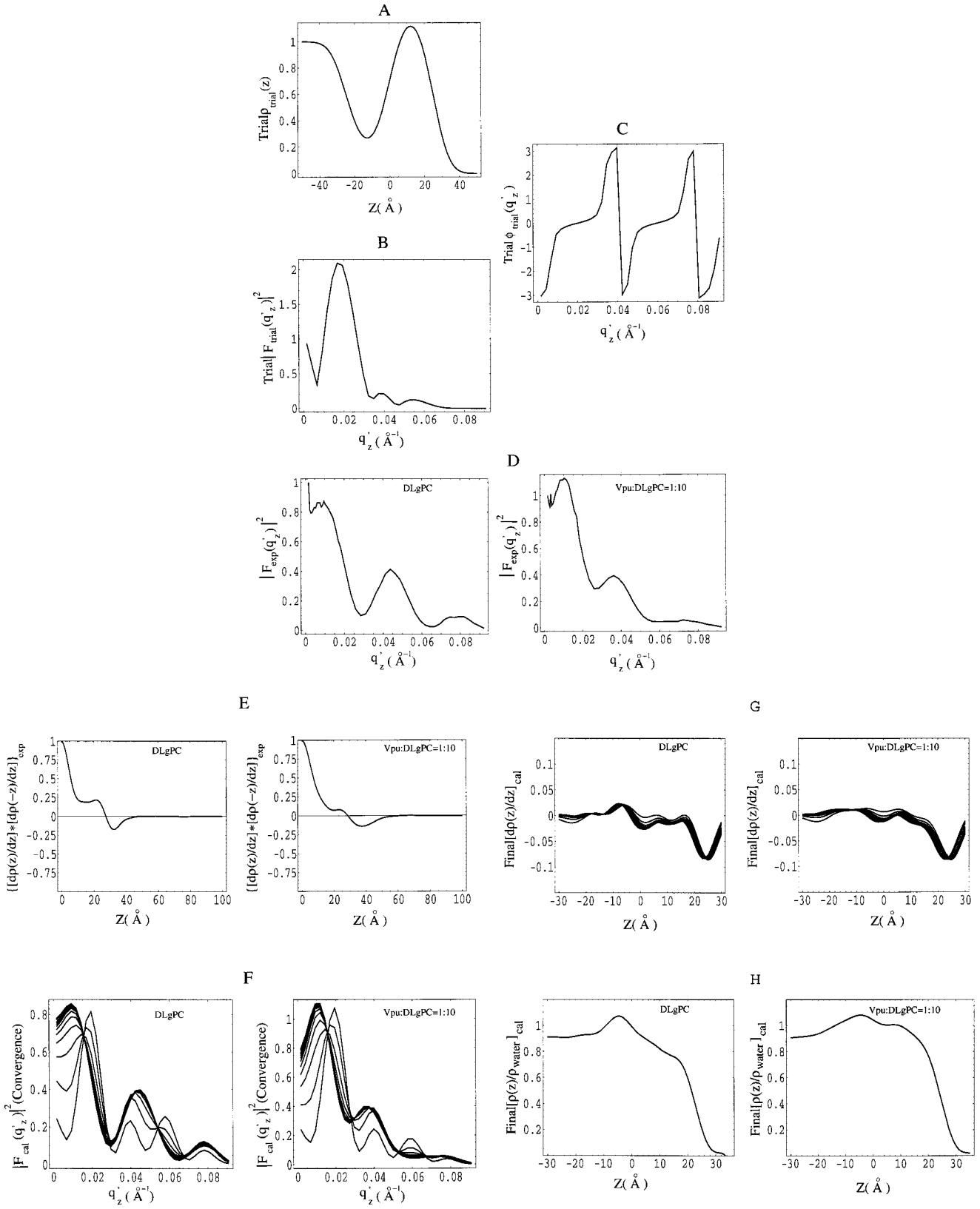

FIGURE 7 Illustration of the box-refinement method of analysis for normalized reflectivity data from Langmuir monolayers. (*A*) Trial electron density profile $\rho_{trial}(z)$ used to initiate the box refinement. (*B*) Modulus square $|F_{trial}(q_z')|^2$ of the Fourier transform of the derivative $[d\rho_{trial}(z)/dz]$ as a function of photon momentum transfer q_z'. (*C*) Phase $\phi_{trial}(q_z')$ of the Fourier transform of the derivative $[d\rho_{trial}(z)/dz]$ as a function of photon momentum transfer q_z'. Only this trial phase function originating from the trial electron density profile $\rho_{trial}(z)$ is used to initiate the box refinement. (*D*) Experimental normalized

refinement is most convincing when a number of different trial profile structures converge to the same resultant profile structure, or when an obviously incorrect trial structure converges to a resultant profile fully consistent with our physical–chemical knowledge of the system. Here we have used an obviously incorrect trial profile structure for the DLgPC monolayer, which did converge to the known profile structure for such diacylphosphatidylcholine monolayers/bilayers. The same trial profile structure was also used in the box-refinement of the normalized reflectivity data from the various Vpu/DLgPC mixtures. In the following, we provide an example of the box-refinement analysis of normalized reflectivity data for DLgPC and Vpu/DLgPC = 1:10 at 45 mN/m.

The initial trial $\rho_{trial}(z)$, selected to be obviously incorrect (namely an excessively broad, relatively electron-deficient "polar headgroup" layer and a broad, relatively electron-rich "hydrocarbon chain" layer) shown in Fig. 7 *A* was used to initiate the box-refinement. The Fourier transform of the derivative of the initial trial $\rho_{trial}(z)$, namely $FT[d\rho/dz]_{trial}$, provides the modulus and the required initial phase function. The square of this modulus (see Fig. 7 *B*) compares very poorly with the experimental modulus squared $|R_{exp}(q_z)/R_F(q_z)|^2$ expressed in q_z'-space as $|F_{exp}(q_z')|^2$ (see Fig. 7 *D*). At this step, the agreement is poor because the initial trial $\rho_{trial}(z)$ was purposely chosen to be incorrect. We then use the trial phase function (see Fig. 7 *C*) to compute the inverse Fourier transform of the experimental modulus $|F_{exp}(q_z')|$ and obtain a new derivative $(d\rho/dz)_1$. This new derivative of the electron density profile generally contains significant features well beyond the finite extent of the actual profile structure for the monolayer. At this point, we first use the box constraint, namely the known finite extent of the monolayer profile structure. The box size is obtained by computing the inverse Fourier transform of the experimental normalized reflectivity data, $FT^{-1}[|F_{exp}(q_z')|^2]$, which is simply the autocorrelation of $d\rho(z)/dz$, namely $\{(d\rho(z)/dz) * (d\rho(-z)/dz)\}_{exp}$, as shown in Fig. 7 *E*. The autocorrelation, or generalized Patterson function, shows no significant features beyond $z \sim 50-60$ Å, the maximal extent of the actual profile structure of the monolayer. The new derivative of the electron density $(d\rho/dz)_1$ is then set to zero outside a 60-Å-wide region centered on the $z = 0$ Å origin, as defined solely by the arbitrary positioning of the initial trial profile structure along the *z*-axis, to generate a truncated derivative of the electron density profile $(d\rho/dz)_{1t}$. This $(d\rho/dz)_{1t}$ becomes the new trial profile structure in the next iteration of the refinement. The procedure is repeated until the square of the modulus of the Fourier transform of the so-iterated derivative of the electron density profile converges to the experimental $R_{exp}(q_z)/R_F(q_z)$ data expressed in q_z'-space as $|F_{exp}(q_z')|^2$ to within the counting statistics noise. Figure 7 *F* shows the procedure for the iterations 1–10, 20, 30, 40, and 50. It can be seen that the refinement converges, progressing from the totally incorrect modulus square from the initial trial profile (Fig. 7 *B*) to the experimental $|F_{exp}(q_z')|^2$ data (Fig. 7 *D*) in about ten iterations. Fig. 7 *G* shows corresponding convergence from the clearly incorrect trial $d\rho/dz$ to the fully converged $d\rho/dz$. The integration of the fully converged $d\rho/dz$ provides the final electron density profile $\rho(z)$ itself (see Fig. 7 *H*), which exhibits the expected features of a diacylphosphatidylcholine monolayer for the DLgPC case as described above in slab model. Similarly, the electron density profiles obtained via box-refinement according to the above procedure using the same initial trial electron density profile for all mole ratios of Vpu/DLgPC at the pressure 45 mN/m and for the 1:10 mole ratio of Vpu/DLgPC at pressures 13, 45, and 55 mN/m are shown in Fig. 8 and Fig. 9, respectively. It can be seen, from inspection of Fig. 5 compared with Fig. 8, and Fig. 6 compared with Fig. 9, that the general features of these electron density profiles obtained via box-refinement are qualitatively the same as those obtained via model refinement, however the profiles do differ somewhat in detail (see below).

DISCUSSION

Using the slab model-refinement approach, one is forced to assume a finite number of slabs or steps in the initial model profile representative of one's physical–chemical knowledge of the monolayer system under study. Although this can be relatively straightforward for pure monolayers composed of a relatively simple molecular component (e.g., a particular fatty-acid or phospholipid), it is not for more complex components possessing a greater number of internal degrees of freedom. This is further complicated, especially for mixtures, by the fact that these slabs or steps must average over in-plane structure of the monolayer via the projection of its 3D structure onto the profile *z*-axis normal to the monolayer plane. The maximum number of slabs or steps is dictated by the range of momentum transfer q_z covered by the reflectivity data and its inherent errors in-

reflectivity $R(q_z')/R_F(q_z')$ expressed as a function of photon momentum transfer q_z', $|F_{exp}(q_z')|^2$. (*E*) Inverse Fourier transform of the experimental $|F_{exp}(q_z')|^2$, which provides the autocorrelation of the derivative of the electron density profile $\{[d\rho_{exp}(z)/dz] * [d\rho_{exp}(-z)/dz]\}$ for the monolayer. The box constraint, key input to the box-refinement analysis, was chosen to be $L = 60$ Å, well beyond the last significant feature a $z \sim 40$ Å. (*F*) The convergence of the calculated $|F(q_z')|^2$ from the box refinement to the experimental $|F_{exp}(q_z')|^2$ for iterations 1–10, 20, 30, 40, and 50. (*G*) The convergence of the calculated $d\rho(z)/dz$ from the box refinement to the final $d\rho_{exp}(z)/dz$ for iterations 1–10, 20, 30, 40, and 50. (*H*) The integration of the final converged $d\rho(z)/dz$ to the electron density profile for the monolayer $\rho_{exp}(z)$ itself.

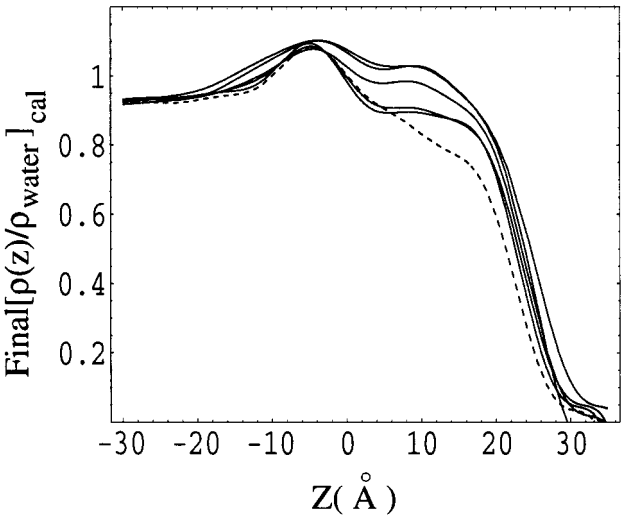

FIGURE 8 Electron density profiles obtained from the box-refinement analysis as a function of increasing Vpu/DLgPC mole ratio at a surface pressure of 45 mN/m and $T = 20°C$. These profiles should be compared with those from the model refinement analysis shown in Fig. 5. Pure DLgPC is in dashed line. Mixed monolayer over the range of Vpu/DLgPC mole ratio of 1:50, 1:40, 1:20, 1:15, and 1:10 are represented in solid lines. As the mole ratio increases, the electron density increase.

cluding counting statistics. Generally, only the smallest number of slabs or steps necessary to achieve agreement with the experimental normalized reflectivity data is believable. Conversely, this minimal number of slabs or steps does not appear so explicitly in the box-refinement approach. Instead, a continuous electron density profile is generated that is fully consistent with the experimental reflectivity data. Features can thereby appear in the profile without having to assume their existence at the outset. Nevertheless, the interpretation of these profiles in terms of the monolayer's molecular components and their possible 3D structures must be consistent with the same considerations described above.

The electron density profiles derived from the normalized reflectivity data for the mixed Vpu/DLgPC monolayers, both as a function of mole ratio at constant surface pressure and as a function of surface pressure at constant mole ratio, using two unrelated methods are in good qualitative agreement. Given that there are a finite number of equally good mathematical solutions to the phase problem for the generally asymmetric profile structures of such Langmuir monolayers, this agreement is key to establishing the so-derived profile structures as the physically correct structures. Thus, the slab model-refinement approach, as applied here, has indeed converged to the correct solution for the monolayer electron density profile for the cases studied providing the basis for the interpretation of these profiles in terms of their molecular components as presented below.

We first consider the profiles shown in Fig. 5 for the mixed Vpu/DLgPC monolayers as a function of increasing mole ratio at a constant, relatively high surface pressure of 45 mN/m. It is readily apparent that increasing the Vpu content of the monolayer has two major effects on the monolayer electron density profile. One major effect is a systematic increase in the width of the relatively electron-dense feature ($-10\ Å < z < 0\ Å$) associated with the phospholipid headgroups in the pure DLgPC monolayer. This increase is localized to an approximately 10-Å-wide region (again using the half maximal points as in Fig. 4) on the water subphase side of the polar headgroups ($z < -10\ Å$). Because the cross-sectional diameter of α-helices is $\sim$10 Å and their unhydrated electron density is $\sim$0.521 e/Å^3 (relative to $\sim$0.385 e/Å^3 at 45 Å/molecule for the DLgPC headgroups and 0.333 e/Å^3 for bulk water), it is reasonable to assume that the amphipathic helices of Vpu's cytoplasmic domain cause this increase in electron density by lying on the surface of the DLgPC polar headgroups. The smaller systematic increase in electron density associated with the polar headgroups in the pure DLgPC monolayer may be due to the displacement of water from the headgroup layer by the side-chains of the helices. Conversely, if the helices associated with Vpu's cytoplasmic domain were fully extended normal to the plane of the DLgPC polar headgroup surface, their in-plane concentration even at the highest Vpu/DLgPC mole ratio of 1:10 remains too low to significantly increase the electron density of the water subphase, and they would therefore be unobservable in the monolayer electron density profile. The second major effect is a systematic increase in the width and electron density of the relatively electron-deficient feature ($0\ Å < z < 30\ Å$) associated with the phospholipid hydrocarbon chains in the pure DLgPC monolayer. Given the calculated electron density ($\sim$0.491 e/Å^3) and length ($\sim$34 Å) of the unhydrated transmembrane α-helix of Vpu as compared to the calculated electron density (0.281 e/Å^3 at 45 Å^2/molecule) and maximal length ($\sim$30 Å) of the DLgPC hydrocarbon chains, it is reasonable to assume that the hydrophobic transmembrane helix, oriented approximately normal to the monolayer plane, is responsible for observed effects the (increased electron density and length). This would account quantitatively for both the maximal increase in electron density to $\sim$0.34 e/Å^3 in the region of overlap of the chains and helices ($0\ Å < z < 30\ Å$) at the largest Vpu/DLgPC mole ratio of 1:10, as well as the excess electron density for $z > 30$ Å at the higher mole ratios. Based on the above analysis of the electron density profiles for the mixed Vpu/DLgPC monolayers at a constant surface pressure of 45 mN/m, the profile structure of the mixed Vpu/DLgPC monolayers on the water surface can be well described by the schematic model shown in Fig. 10. The amphipathic α-helices lie on the surface of the phospholipid headgroups without extending further into the bulk water subphase. The hydrophobic α-helix is oriented approximately perpendicular to the plane of monolayer within the phospholipid hydrocarbon chain layer. Note that all of the effects described

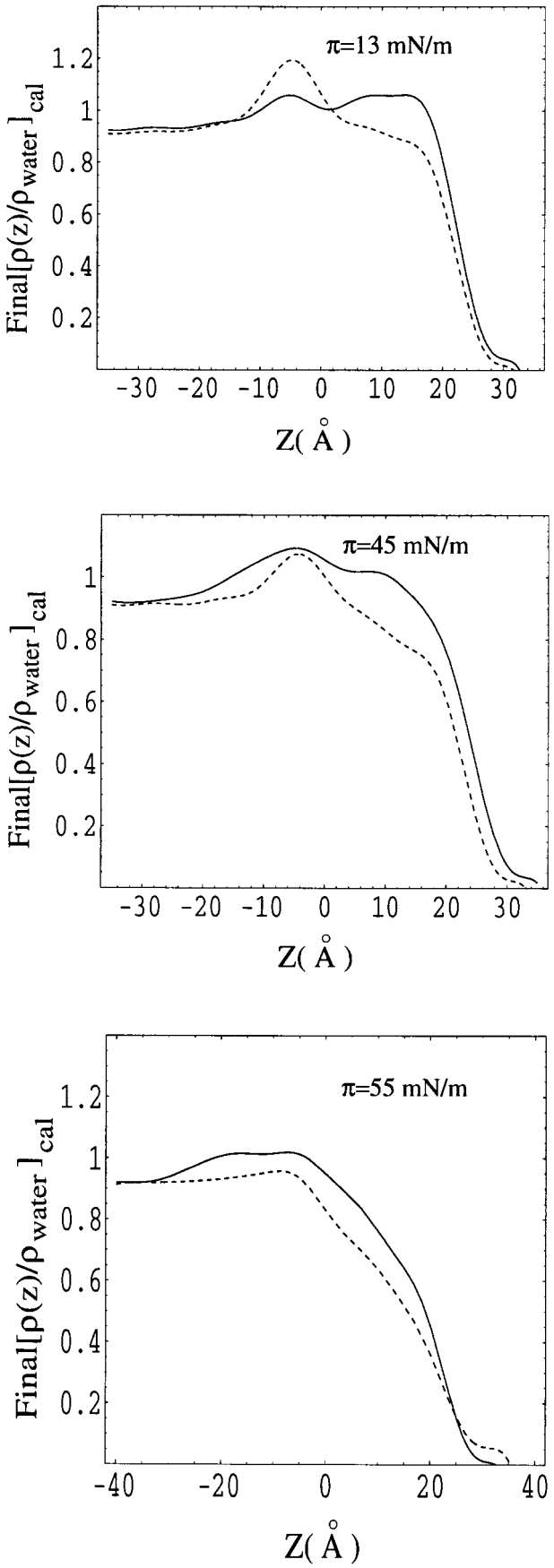

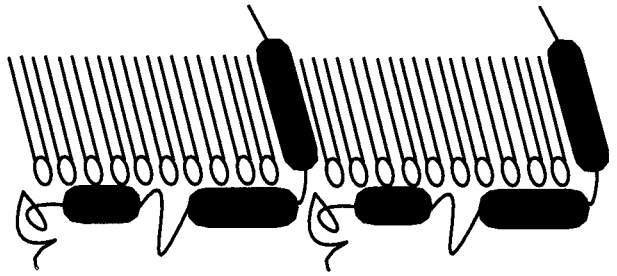

FIGURE 10 Schematic showing the known secondary structure of Vpu incorporated into the host DLgPC monolayer to be fully consistent with the electron density profiles derived in this work for the various mixed monolayers over the range of Vpu/DLgPC mole ratios of 1:∞, 1:50, 1:40, 1:20, 1:15, and 1:10 at a surface pressure of 45 mN/m and $T = 20$°C.

in this paragraph are also observed in the corresponding profiles derived independently via box refinement (Fig. 8). In fact, they may be better observed in these profiles because no assumptions were required concerning the number of interfaces in the monolayer profile structure, as was the case for those obtained via model refinement (Fig. 5).

We next consider the profiles shown in Fig. 6 for the mixed Vpu/DLgPC monolayers at a maximal mole ratio of 1:10 as a function of surface pressure. First note that the interpretation of the electron density profile for the mixed Vpu/DLgPC monolayer at this maximal mole ratio and the surface pressure of 45 mN/m was discussed in the previous paragraph, and the lower (13 mN/m) and higher (55 mN/m) surface pressure cases will be discussed relative to the 45 mN/m case. At the substantially lower surface pressure of 13 mN/m, the profile structure of pure DLgPC contains distinct and well-defined polar headgroup (-10 Å $< z <$ 0 Å) and hydrocarbon chain (0 Å $< z <$ 20 Å) features. The shortness of the hydrocarbon chain region, compared to the extended all-trans length of the DLgPC hydrocarbon chains ($\sim$30 Å), together with the relative sharpness of the hydrocarbon–air interface, suggests that the hydrocarbon chains are substantially more tilted with respect to the normal to the monolayer plane, consistent with a larger area per molecule in the monolayer plane at this relatively low surface pressure. As can be seen, the incorporation of Vpu, at this maximal mole ratio and surface pressure. As can be seen, the incorporation of Vpu, at this maximal mole ratio and surface pressure below the "kink" in the pressure/area isotherm, again has two major effects on the profile structure of the host DLgPC monolayer, as compared with the higher pressure of 45 mN/m discussed in the paragraph above. The

FIGURE 9 Electron density profiles obtained from the box-refinement analysis for pure DLgPC (*dashed line*) and the 1:10 mole ratio of Vpu/DLgPC (*solid line*) at surface pressures of (*A*) 13 mN/m, (*B*) 45 mN/m, and (*C*) 55 mN/m and $T = 20$°C. These profiles should be compared with those from the model-refinement analysis shown in Fig. 6.

first effect is a substantial decrease in the electron density of the phospholipid headgroup region (-10 Å $< z < 0$ Å) with little broadening of this feature. This may arise simply from the increased area per molecule at this lower surface pressure, allowing more water to be associated with the headgroups. In addition, unlike the higher pressure cases, there appears to be no excess electron density on the surface of the headgroups associated with the amphipathic helices of the cytoplasmic domain. The second effect is again a dramatically increased electron density of the hydrocarbon chain region due to the presence of the transmembrane helix, but higher in density and confined to a narrower region of the profile structure (0 Å $< z <$ 25 Å) as compared with 45 mN/m pressure, consistent with a substantial tilt of the transmembrane helix with respect to the monolayer normal, namely, ~48°. This increased tilt of the transmembrane helix could be responsible for the "disappearance" of the cytoplasmic domain's amphipathic helices from the monolayer electron density profile. The loop connecting the transmembrane helix to the first amphipathic helix of the cytoplasmic domain is very short and probably highly constrained in conformation, because it is composed of only three residues (EYR), the side-chains of the first and third residues being oppositely charged with an intervening residue with a bulky side chain. Thus the increased tilt of the transmembrane helix at this lower surface pressure could force the amphipathic helices off the surface of the polar headgroups into the subphase. Even if they remain coiled, they would not change the electron density of the water subphase if they extend away from the headgroups at this mole ratio and there is recent evidence from nuclear magnetic resonance spectroscopy that the helices of the cytoplasmic domain may uncoil in bulk water (Ma and Opella, 2000) rendering them even less visible in the monolayer electron density profile. These two possibilities are shown schematically in Fig. 11 *A*. At the higher surface pressure of 55 mN/m, the profile structure of the pure DLgPC monolayer is strongly disordered, as can be seen from the substantial broadening of all the interfaces (water–headgroup, headgroup–hydrocarbon chain, and hydrocarbon chain–air), as compared with the lower pressure cases. At this highest surface pressure, this most likely arises from a disordering of the DLgPC molecules along the profile *z*-axis. In this case, the incorporation of Vpu into the host DLgPC monolayer at this maximal mole ratio has the most pronounced effect on the amphipathic helices of the cytoplasmic domain. Their higher electron density relative to that of the water subphase is now seen to extend ~20 Å from the aqueous surface of the DLgPC headgroups, some 10 Å further into the subphase than for the lower 45 mN/m surface pressure case. According to the pressure/area isotherms for pure DLgPC as shown in Fig. 1, the area per molecule is only 40 Å^2 at pressure of 55 mN/m versus 45 Å^2 at 45 mN/m. 10 DLgPC molecules thereby provide a surface area of only 400 Å^2 at 55 mN/m as compared with 450 Å^2 at 45 mN/m. Because the area required for the two amphipathic α-helices of Vpu to lie on the surface of the polar headgroups is calculated to be ~450 Å^2, the higher surface pressure of 55 mN/m may force the second amphipathic helix to lie somewhat further away from the surface of the headgroups. However, the secondary structures of amphipathic helices have, by definition, a hydrophilic side and hydrophobic side. Thus, the hydrophobic sides could associate in a polar environment to form a two-helix bundle approximately 10 × 20 Å, as depicted in the schematic shown in Fig. 11 *C*, while still maintaining their association with the polar headgroup surface consistent with the well-defined 20-A-wide region of relatively high electron density on the surface of the polar headgroups. Again, note that all of the effects described in this paragraph are also observed in the corresponding profiles derived independently via box refinement (Fig. 9). In fact, they are more likely better

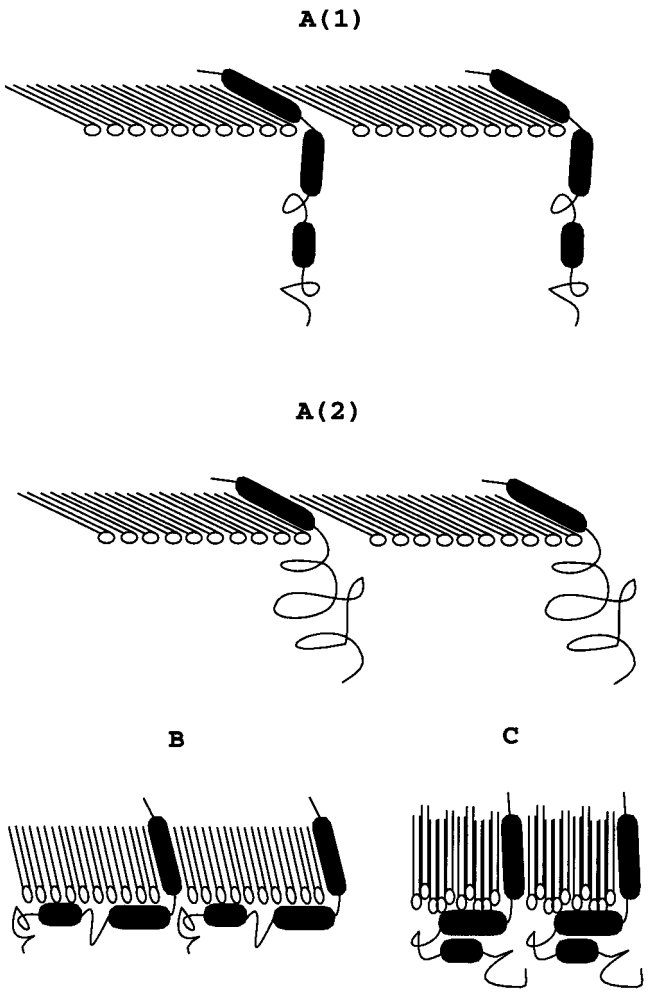

FIGURE 11 Schematic showing the known secondary structure of Vpu incorporated into the host DLgPC monolayer to be fully consistent with the electron density profiles derived in this work for the mixed monolayer at a Vpu/DLgPC mole ratio of 1:10 and surface pressures of (*A*) 13 mN/m, (*B*) 45 mN/m, and (*C*) 55 mN/m and $T = 20$°C.

observed in these profiles because no assumptions were required concerning the number of interfaces in the monolayer profile structure, as was the case for those obtained via model refinement (Fig. 6).

CONCLUSIONS

The synchrotron radiation-based x-ray reflectivity technique has been applied to mixed Langmuir monolayers of the HIV-1 accessory protein Vpu and the long-chain diacyl phospholipid DLgPC. These mixed monolayers were studied as a function of mole ratio at constant surface pressure and as a function of surface pressure at maximal protein/lipid mole ratio. The two components were found to mix over the ranges of protein/lipid mole ratios and surface pressures studied, in spite of the saturated long-chain diacyl phospholipid used. The electron density profiles for these monolayers were derived by two independent methods, ensuring the physical correctness of the profiles so-derived. The hydrophobic α-helix of Vpu's transmembrane domain was found to be localized in the hydrocarbon chain layer of the host phospholipid monolayer independent of variation in protein/lipid mole ratio, but its tilt angle with respect to the normal to the monolayer plane was found to be strongly dependent on surface pressure, decreasing with increasing pressure between 13 and 45 mN/m. Both amphipathic α-helices of Vpu's cytoplasmic domain were found to lie on the surface of the phospholipid headgroups for surface pressures at 45 mN/m. In contrast, the larger tilt angle of the transmembrane helix at the lower surface pressure of 13 mN/m appears to have resulted in forcing the amphipathic helices to extend away from the surface of headgroups into the bulk water subphase, possibly due to the short and restrictive EYR loop connecting the transmembrane helix and the first helix of the cytoplasmic domain. At the highest surface pressure of 55 mN/m, where there was insufficient area to allow both amphipathic helices to lie on the surface of the phospholipid headgroups, the second helix being forced off the surface of the polar headgroups to form a two-helix bundle.

Future x-ray scattering studies of this system in the form of such Langmuir monolayers will use 1) other phospholipids, including those exhibiting a liquid–crystalline phase in pure form; 2) the submolecular fragments of Vpu, namely its hydrophobic transmembrane domain (residues 2–51) and its hydrophilic cytoplasmic domain (residues 28–81); and 3) the phosphorylation of its cytoplasmic domain critical to Vpu's function. Grazing-incidence x-ray diffraction will also be used to investigate the in-plane aggregation (or "oligomeric") state of the transmembrane domain, presumably key to Vpu's cation channel activity. Finally, neutron reflectivity experiments using Vpu with selectively deuterium-labeled residues will be used to investigate the more detailed interaction of the cytoplasmic domain with the phospholipid headgroups.

We thank Elaine Dimasi and Scott Coburn for assistance with the instrumental alignment of the beamline X22B at NSLS; Andrey Tronin, Larry Kneller, Ann Edwards, Erik Nordgren, and Shixin Ye for assistance with data collection; and Dr. David Vaknin for the use of his Langmuir trough.

This research was supported by National Institute of General Medical Science Program Project Grant PO1 GM56538.

REFERENCES

Als-Nielsen, J., and P. S. Pershan. 1983. Synchrotron x-ray diffraction study of liquid surface. *Nucl. Instrum. Meth.* 208:545–548.

Als-Nielsen, J., D. Jacquemain, K. Kjaer, F. Leveiller, M. Lahav, and L. Leiserowitz. 1994. Principles and applications of grazing-incidence X-ray and neutron scattering from ordered molecular monolayers at the air–water interface. *Physics Rep.* 246:251–313.

Bevington, P. R., and D. K. Robinson. 1992. Data Reduction and Error Analysis for the Physical Sciences, McGraw-Hill, Inc, New York.

Blasie, J. K., and P. Timmins. 1999. Neutron scattering in structural biology and biomolecular materials. *MRS Bull.* 24:40–47.

Bour, S., U. Schuber, and K. Strebel. 1995. The human immunodeficiency virus type 1 Vpu protein specifically binds to the cytoplasmic domain of CD4: implications for the mechanism of degradation. *J. Virol.* 69: 1510–1520.

Braslau, A., P. S. Pershan, G. Swislow, B. M. Ocko, and J. Als-Nielsen. 1988. Capillary waves on the surface of simple liquids measured by x-ray reflectivity. *Phys. Rev. A.* 38:2457–2470.

Chen, M., F. Maldarelli, M. K. Karczewski, R. L. Willey, and K. Strebel. 1993. Human immunodeficiency virus type 1 Vpu protein induces degradation of CD4 in vitro: the cytoplasmic domain of CD4 contributes to Vpu sensitivity. *J. Virol.* 67:3877–3884.

Emerman, M., and H. M. Malim. 1998. HIV-1 regulatory/accessory genes: keys to unraveling viral and host cell biology. *Science.* 280:1880–1884.

Ewart, G. D., T. Sutherland, P. W. Gage, and G. B. Cox. 1996. The Vpu protein of human immunodeficiency virus type 1 forms cation-selective ion channels. *J. Virol.* 70:7108–7115.

Federau, T., U. Schubert, J. Flobdorf, P. Henklein, D. Schomburg, and V. Wray. 1996. Solution structure of the cytoplasmic domain of the human immunodeficiency virus type 1 encoded virus protein U (Vpu). *Int. J. Peptide Protein Res.* 47:297–310.

Gross, E., and B. Witkop. 1961. Selective cleavage of methionyl peptide bonds in ribonuclease with cyanogen bromide. *J. Am. Chem. Soc.* 83:1822–1832.

Helm, C. A., H. Möhwald, K. Kjaer, and J. Als-Nielsen. 1987. Phospholipid monolayer density distribution perpendicular to the water surface. A synchrotron x-ray reflectivity study. *Europhys. Lett.* 4:697–703.

Helm, C. A., P. Tippmann-Krayer, H. Möhwald, J. Als-Nielsen, and K. Kjaer. 1991. Phases of phosphatidyl ethanolamine monolayers studied by synchrotron x-ray scattering. *Biophys. J.* 60:1457–1476.

Ionov, R., A. El-Abed, A. Angelova, M. Goldmann, and P. Peretti. 2000. Asymmetrical ion-channel model inferred from two-dimensional crystallization of a peptide antibiotic. *Biophys. J.* 78:3026–3035.

Kjaer, K., J. Als-Nielsen, C. A. Helm, P. Tippmann-Krayer, and H. Möhwald. 1989. Synchrotron x-ray diffraction and reflection studies of arachidic acid monolayers at the air–water interface. *J. Phys. Chem.* 93:3200–3206.

Lösche, M., M. Piepenstock, A. Diedrich, T. Grünewald, K. Kjaer, and D. Vaknin. 1993. Influence of surface chemistry on the structural organization of macromolecular protein layers adsorbed to functionalized aqueous interfaces. *Biophys. J.* 65:2160–2177.

Lenburg, M. E., and N. R. Landau. 1993. Vpu-induced degradation of CD4: requirement for specific amino acid residues in the cytoplasmic domain of CD4. *J. Virol.* 67:7238–7245.

Ma, C., and S. J. Opella. 2000. Lanthanide ions bind specifically to an added "EF-hand" and orient a membrane protein in micelles for solution NMR spectroscopy. *J. Magn. Reson.* 146:380–384.

Maierhofer, A. P., D. G. Bucknall, and T. M. Bayerl. 2000. Modulation of cytochrome *c* coupling to anionic lipid monolayers by a change in phase state: a combined neutron and infrared reflection study. *Biophys. J.* 79:1428–1437.

Majewski, J., T. L. Kuhl, K. Kjaer, M. C. Gerstenberg, J. Als-Nielsen, J. N. Israelachvili, and S. Smith. 1998. X-ray synchrotron study of packing and protrusions of polymer-lipid monolayers at the air–water interface. *J. Am. Chem. Soc.* 120:1469–1473.

Makowski, L. 1981. The use of continuous diffraction data as a phase constraint. I. One-dimensional theory. *J. Appl. Cryst.* 14:160–168.

Maldarelli, F., M. Chen, R. L. Willey, and K. Strebel. 1993. Human immunodeficiency virus type 1 Vpu protein is an oligomeric type I integral membrane protein. *J. Virol.* 67:5056–5061.

Marassi, F. M., C. Ma, H. Gratkowski, S. K. Straus, K. Strebel, M. Oblatt-Montal, M. Montal, and S. J. Opella. 1999. Correlation of the structural and functional domains in the membrane protein Vpu from HIV-1. *PNAS.* 96:14336–14341.

Möhwald, H. 1995. Phospholipid monolayers. *In* Structure and Dynamics of Membranes. R. Lipowsky and E. Sackmann, editors. Elsevier Science B.V., Amsterdam. 161–211.

Ocko, B. M., X. Z. Wu, E. B. Sirota, S. K. Sinha, O. Gang, and M. Deutsh. 1997. Surface freezing in chain molecule: normal alkanes. *Phys. Rev. E.* 55:3164–3182.

Schubert, U., S. Bour, A. V. Ferrer-Montiel, M. Montal, F. Maldarelli, and K. Strebel. 1996. The two biological activities of human immunodeficiency virus type 1 Vpu protein involve two separable structure domains. *J. Virol.* 70:809–819.

Schubert, U., and K. Strebel. 1994. Differential activities of the human immunodeficiency virus type 1-encoded Vpu protein are regulated by phosphorylation and occur in different cellular compartments. *J. Virol.* 68:2260–2271.

Schubert, U., P. Henklein, B. Boldyreff, E. Wingender, K. Strebel, and T. Porstmann. 1994. The human immunodeficiency virus type 1 encoded Vpu protein is phosphorylated by casein kinase-2 (CK-2) at positions Ser52 and Ser56 within a predicted alpha-helix-turn-alpha-helix-motif. *J. Mol. Biol.* 236:16–25.

Schwarz, G., and S. E. Taylor. 1999. Polymorphism and interactions of a viral fusion peptide in a compressed lipid monolayer. *Biophys. J.* 76: 3167–3175.

Shapovalov, V. L., E. A. Kotova, T. I. Rokitskaya, and Y. N. Antonenko. 1999. Effect of gramacidin A on the dipole potential of phospholipid membranes. *Biophys. J.* 77:299–305.

Skita, V., M. Filipkowski, A. F. Garito, and J. K. Blasie. 1986a. Profile structure of very thin multilayers by x-ray diffraction using direct and refinement methods of analysis. *Phys. Rev. B.* 34:5826–5837.

Skita, V., W. Richardson, M. Filipkowski, A. Garito, and J. K. Blasie. 1986b. Overlayer-induced ordering of the disordered surface monolayer in Langmuir–Blodgett multilayer thin films. *J. Physique.* 47:1849–1855.

Stroud, R. M., and D. A. Agard. 1979. Structure determination of asymmetric membrane profiles using an iterative Fourier method. *Biophys. J.* 25:495–512.

Strzalka, J., X. Chen, C. C. Moser, P. L. Dutton, B. M. Ocko, and J. K. Blasie. 2000. X-ray structure studies of maquette peptide monolayers 1. Reflectivity and G10 at the air/water interface. *Langmuir*. 16: 10404–10418.

Tidswell, I. M., B. M. Ocko, P. S. Pershan, S. R. Wasserman, G. M. Whitesides, and J. D. Axe. 1990. X-ray specular reflection studies of silicon coated by organic monolayers (alkylsiloxanes). *Phys. Rev. B.* 41:1111–1128.

Willey, R. L., F. Maldarelli, M. Martin, and K. Strebel. 1992. Human immunodeficiency virus type 1 Vpu protein induces rapid degradation of CD4. *J. Virol.* 66:7193–7200.

Willbold, D., S. Hoffmann, and P. Rösch. 1997. Secondary structure and tertiary fold of the human immunodeficiency virus protein U (Vpu) cytoplasmic domain in solution. *Eur. J. Biochem.* 245:581–588.

Wray, V., T. Federau, P. Henklein, S. Klabunde, O. Kunert, D. Schomburg, and U. Schubert. 1995. Solution structure of the hydrophilic region of HIV-1 encoded virus protein U (Vpu) by CD and ^{1}H NMR spectroscopy. *J. Peptide Protein Res.* 45:35–43.